Supramolecular Chemistry
Publication details, including instructions for authors and subscription information:
http://www.informaworld.com/smpp/title~content=t713649759

Silver Containing Nanostructures from Hydrogen-bonded Supramolecular Scaffolds

S. Kinge[a]; M. Péter[a]; M. Crego-calama[a]; D. N. Reinhoudt[a]
[a] Laboratory of Supramolecular Chemistry and Technology, MESA+ Institute for Nanotechnology, University of Twente, Enschede, The Netherlands

To cite this Article Kinge, S. , Péter, M. , Crego-calama, M. and Reinhoudt, D. N.(2008) 'Silver Containing Nanostructures from Hydrogen-bonded Supramolecular Scaffolds', Supramolecular Chemistry, 20: 6, 593 — 600

To link to this Article: DOI: 10.1080/10610270701537888

URL: http://dx.doi.org/10.1080/10610270701537888

Supramolecular Chemistry, September 2008 Vol. 20 (6), pp. 593–600

Silver Containing Nanostructures from Hydrogen-bonded Supramolecular Scaffolds

S. KINGE, M. PÉTER, M. CREGO-CALAMA* and D. N. REINHOUDT

Laboratory of Supramolecular Chemistry and Technology, MESA$^+$ Institute for Nanotechnology, University of Twente, PO Box 217, 7500 AE Enschede, The Netherlands

(Received 9 May 2007; Accepted 23 June 2007)

The self-organisation of silver-containing hydrogen-bonded rosette assemblies on highly oriented pyrolytic graphite (HOPG) surfaces is described. The introduction of silver atoms into the double rosette architecture was achieved using the affinity of silver cations for cooperative π-donors or cyano functionalities on the double rosettes. Highly ordered 2-D nanorod domains with an inter-row spacing of 4–5 nm oriented in different directions were revealed by tapping-mode atomic force microscopy (AFM). This new and simple strategy for the creation of metal-containing supramolecular nanorod arrays that can act as well-defined surface-immobilised self-assembled scaffolds, will contribute to the development of functionalised nanoarchitectures via bottom–up approaches.

Keywords: Hydrogen-bonds; Supramolecular chemistry; Self-assembly; Templation-silver complexation; Nano-domains

INTRODUCTION

Self-assembly and self-organisation of small building blocks is at the heart of bottom–up approaches [1–3] as an alternative to currently employed costly lithography based top–down methods of micro-nanofabrication [4–6] for engineering large-scale ensembles of nanoarchitectures [7–11]. As a natural phenomenon in biological [12] and chemical processes [13–15], self-assembly offers attractive possibilities for creating functional molecular structures, for example artificial molecular machines [16–19]. Recent research interests are focused towards the fabrication, and specially positioning of noncovalent supramolecular aggregates on surfaces in organised networks [20–29]. Though many examples of supramolecular structures formed *in situ* on surfaces are known, only few superstructures formed in solution have been efficiently transferred onto surfaces [20,21,23,24,29–31]. In this line, our group has reported the synthesis and characterisation of multi-component, hydrogen bonded assemblies (rosette) and their ordered rod-like arrangement on the graphite surfaces [32–35]. The rosette assemblies are based on the self-assembly of calix[4]arene dimelamines and barbituric acid (or cyanuric acid) derivatives (Fig. 1), which are held together by complementary hydrogen-bonding between the donor-acceptor-donor (DAD) array of calix[4]arene dimelamine derivatives and the acceptor-donor-acceptor (ADA) array of the BAR (barbituric acid) or CYA (cyanuric acid) counterparts [36–39]. These assemblies can be easily functionalised [40]. Metal-containing self-assembled nanostructures are very interesting for growing metal nanoparticles or creating metallic nanowires from usual biological templates like DNA [41] and peptide nanotubes [42]. Metal atoms bound to the template surface act as nucleating centres for further growth of nanoparticles or can be 'developed' by using standard photographic techniques. In this realm, we have previously achieved the incorporation of gold atoms in the rosette assemblies using coordination to phosphane groups, which are placed on the melamine part of the rosettes as an alternative non-biological pathway for creating metallic structures [34]. However, this pathway includes the multi-step synthesis of gold substituted calix[4]arene dimelamine derivatives, which is a costly and a lengthy process. In this article, we report an alternative pathway of organising metal-containing assemblies

---

*Corresponding author. E-mail: mercedes.cregocalama@imec-nl.nl

ISSN 1061-0278 print/ISSN 1029-0478 online © 2008 Taylor & Francis
DOI: 10.1080/10610270701537888

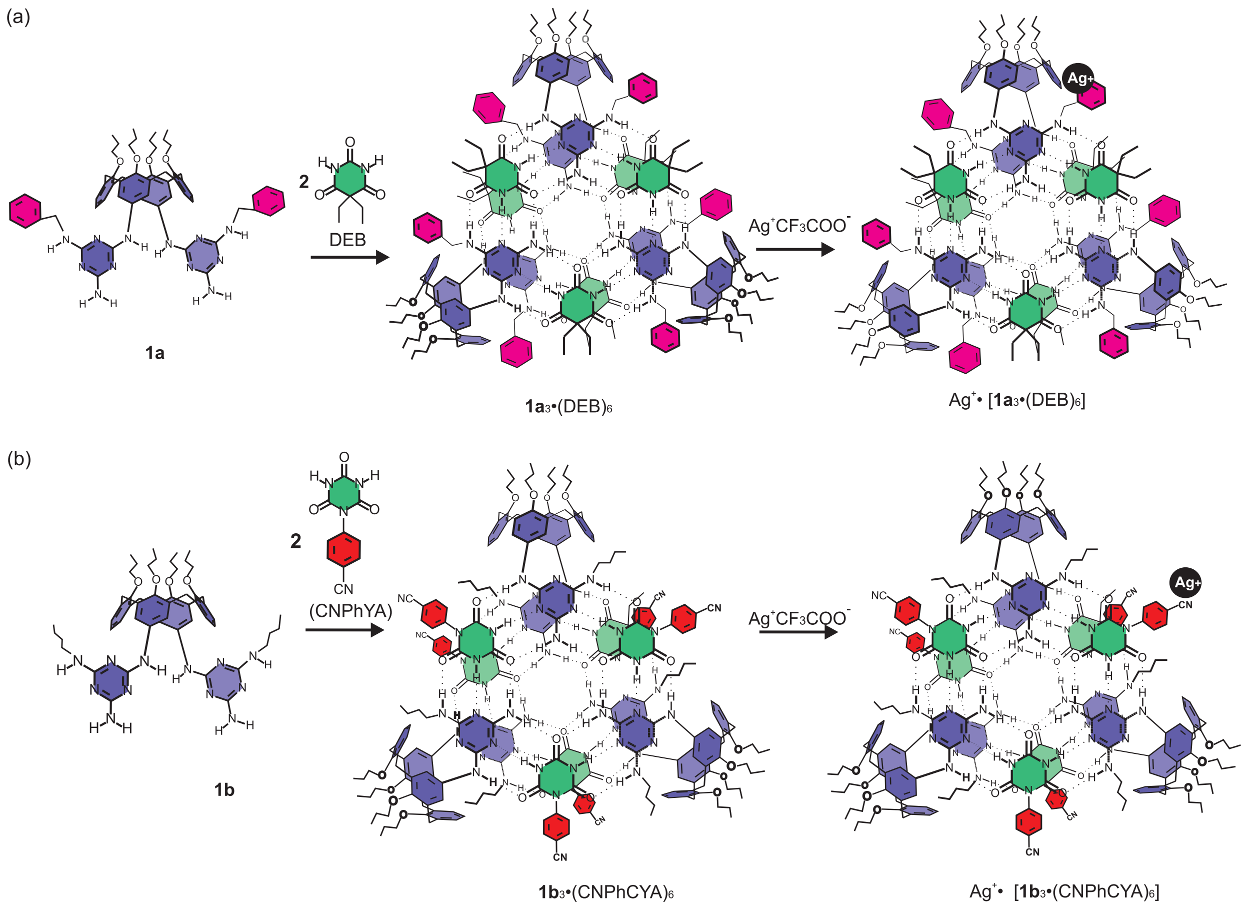

FIGURE 1 Synthesis of silver-functionalised double rosette assemblies Ag^+·[**1a**$_3$•(DEB)$_6$] and Ag^+· [**1b**$_3$•(CNPhCYA)$_6$].

on surfaces without need for multi-step synthesis of metal functionalised precursors. This pathway is based on the use of strong affinity of certain metal ions for example Ag^+ ions for cooperative π-donor or cyano- functionalities easily grafted on the double rosette motifs [43,44].

Here we report the 2-D self-assembly of silver-functionalised double rosette assemblies Ag^+·[**1a**$_3$• (DEB)$_6$] and Ag^+·[**1b**$_3$•(CNPhCYA)$_6$] (Fig. 1) on highly oriented pyrolytic graphite (HOPG) surfaces studied by atomic force microscopy (AFM). AFM is a very versatile and practical method for studying such self-assembled systems on surfaces [36–39]. AFM images show regular 2-D nanorod domains formed from these metal containing supramolecular nanostructures. Different organisations are observed depending upon the building blocks DEB (5,5′-diethyl barbiturate) and CNPhCYA (p-*cyano* phenyl cyanurate). The silver-functionalised double rosette assemblies, Ag^+·[**1a**$_3$•(DEB)$_6$] and Ag^+·[**1b**$_3$•(CNPhCYA)$_6$] were formed [**1a**$_3$•(DEB)$_6$] and [**1b**$_3$•(CNPhCYA)$_6$] double rosette assemblies with $Ag^+CF_3COO^-$. These double rosette assemblies are molecular boxes that consist of two flat and circular self-assembled rosette motifs connected though three calix[4]arene diamelamine moieties via the formation of 36 hydrogen bonds [32–35] (Fig. 1). Employing such templates to direct the formation of metallic nanostructures may lead in the future to versatile routes to fabricate electrically conducting nanowires.

EXPERIMENTAL SECTION

All experiments were performed under argon atmosphere. 5,5′-Diethyl barbiturate (DEB) (Aldrich), 2,5-dihydroxybenzoic acid (DHB) (Aldrich) and $Ag^+CF_3COO^-$ (ACROS) were purchased and used as received. Calix[4]arene dimelamine derivatives **1a**, **1b** and CNPhCYA were synthesised according to the previous protocol. ^{1}H NMR spectra were recorded in $CDCl_3$ on a Varian Unity 300. Chemical shifts are given in ppm relative to tetramethylsilane (TMS). Matrix-Assisted Laser Desorption Ionisation (MALDI) Time-of-Flight (TOF) mass spectra were recorded on a Voyager-DE-RP mass spectrometer (Applied Biosystems/PerSeptive Biosystems, Inc., Framingham, MA, USA) equipped with delayed extraction. A 337 nm UV nitrogen laser producing 3-ns pulses was used and the mass spectra were obtained in the linear and reflectron mode. Tapping mode AFM (TM-AFM) thin-film samples were prepared by deposition of one drop of a solution (0.1 mM) of silver complexed assemblies Ag$^+$·[$\mathbf{1a}_3$•(DEB)$_6$] and Ag$^+$·[$\mathbf{1b}_3$•(CNPhCYA)$_6$] in toluene onto freshly cleaved highly-oriented pyrolytic graphite (HOPG) in a near-saturated atmosphere of toluene. After the solvent was evaporated, the samples were treated for 15 min in oil pump vacuum to remove any traces of residual solvent. The TM-AFM data were acquired with a Nanoscope III multimode AFM (Digital Instruments, Santa Barbara, CA, USA) by using a 10 μm (E) scanner and microfabricated silicon tips/cantilevers (model TESP, resonance frequency of 300 kHz, Nanosensors, Wetzlar, Germany). The system was thermally equilibrated over the period of typically 1 to 2 days by operating the AFM in contact mode with false engagement. The rms amplitude of the cantilever ($\approx$0.8 V) and the amplitude damping ($\approx$5%) were minimised to reduce the peak normal forces. Height, phase, and amplitude images were captured using scan rates between 0.5 Hz and 3.0 Hz. All data presented here have been subject to a first order plane fit to compensate for the sample tilt.

Synthesis of Ag$^+$ Complexes of the Hydrogen-bonded Assemblies [43,44]

5–10 mM solutions of the hydrogen-bonded assemblies [$\mathbf{1a_3}$•(DEB)$_6$] and [$\mathbf{1b_3}$•(CNPhCYA)$_6$] in CHCl$_3$ were stirred for 24 h at room temperature with 1.5 equivalent of Ag$^+$CF$_3$COO$^-$. Further an aliquot of this solution (10 mL) was mixed with an aliquot (30 mL) of a solution of 2,5-dihydroxybenzoic acid (DHB) (3 mgL^{-1}) in CHCl$_3$. A portion (1 mL) of the resulting solution was loaded on a gold-sample plate, the solvent removed in warm air, and the sample transferred to the mass spectrometer for analysis.

RESULTS AND DISCUSSION

Synthesis and Characterisation of Silver-functionalised Double Rosettes

Two different silver-functionalised double rosette assemblies (Fig. 1) were synthesised. The synthesis of double rosette assemblies was performed according to the previous protocol by easily mixing calix[4]arene dimelamine derivatives **1a** (or **1b**) with DEB (5,5-diethyl barbituric acid) or CNPhCYA (*p-cyano*-phenyl cyanuric acid) in 1:2 ratio in apolar solvents: chloroform or toluene [45]. The formation of the assemblies is characterised by ^{1}H NMR. The characteristic signals around 13–15 ppm of hydrogen-bonded imide protons (—NH) on barbituric acid or cyanuric acid derivatives confirm the formation of the double rosette assemblies (Figs. 2b,c). Silver atoms can be easily incorporated in the double rosette assemblies $\mathbf{1a}_3$•(DEB)$_6$ and $\mathbf{1b}_3$•(CNPhCYA)$_6$ by reacting 5–10 mM solution of double rosette assemblies (CHCl$_3$) with 1.5 equivalents of Ag$^+$CF$_3$COO$^-$ for 24 h at room temperature. MALDI-TOF analysis of silver-functionalised assemblies show intense signals in the spectra at m/z = 4278.3 (calcd. 4276.1 for $C_{228}H_{276}N_{48}O_{30}\cdot{}^{107}Ag^+$) for assembly Ag$^+$·[$\mathbf{1a}_3$•(DEB)$_6$] (Fig. 2a) and 4347.9 (calcd. 4348.1 for $C_{222}H_{246}N_{66}O_{42}\cdot{}^{107}Ag^+$) for assembly Ag$^+$·[$\mathbf{1b}_3$• CNPhCYA)$_6$] indicating the incorporation of silver atoms in the rosette architecture [43,44].

Based on literature results, in the assembly Ag$^+$·[$\mathbf{1a}_3$•(DEB)$_6$], the silver ions coordinate to benzyl aromatic ring on calix[4]arene dimelamine presumably forming a sandwich-type complex with the benzyl substituent on the melamine; while in assembly Ag$^+$·[$\mathbf{1b}_3$•(CNPhCYA)$_6$] the silver ion coordinates to the cyano functionalities on the cyanurate derivative [22,46,47]. The introduction of the functional groups in the calix[4]arene dimelamine framework and barbituric/cyanuric acid derivatives can be conveniently performed without interfering with the network of hydrogen bonds that holds the double rosette together.

Atomic Force Microscopy (AFM)

Highly-ordered and regular 2-D arrays of rosette nanostructures were observed after deposition of the rosettes from toluene onto freshly cleaved HOPG surfaces, as unveiled by contact (or tapping) mode AFM (Fig. 3). To suppress the 3-D (bulk) crystallisation of the rosettes, slow evaporation of the solvent in a nearly saturated atmosphere of the solvent was ensured. The AFM data was acquired, as described in detail in experimental section, on a thermally fully equilibrated commercial AFM setup using silicon tips. To prevent sample damage, the rms amplitude of the cantilever and the amplitude damping (5%) were minimised. The observed structure is characterised by an inter-row spacing of 5.1 ± 0.1 nm for assembly Ag$^+$· [$\mathbf{1a}_3$•(DEB)$_6$] (with 1.0 ± 0.2 nm spacing between the neighbouring rosettes) and 4.8 ± 0.1 nm for Ag$^+$· [$\mathbf{1b}_3$•(CNPhCYA)$_6$] (with 1.0 ± 0.1 nm spacing between the neighbouring rosettes). The inter-row spacing or heart-to-heart distance [34] is the separation between two adjacent nanorod structures measured normal to the row direction from centre of one nanorod to another nanorod centre. The observed inter-row distances are a function of the substituents as well as the rosette size and suggests that the rosettes are stacked approximately face-to-face in these rows (Fig. 4) [48]. The silver-functionalised rosettes also show a characteristic roughness of the domain edges. This was prominently observed in case of nanorod domains of assembly Ag$^+$·[$\mathbf{1b}_3$•(CNPhCYA)$_6$]. This is shown in higher-magnification

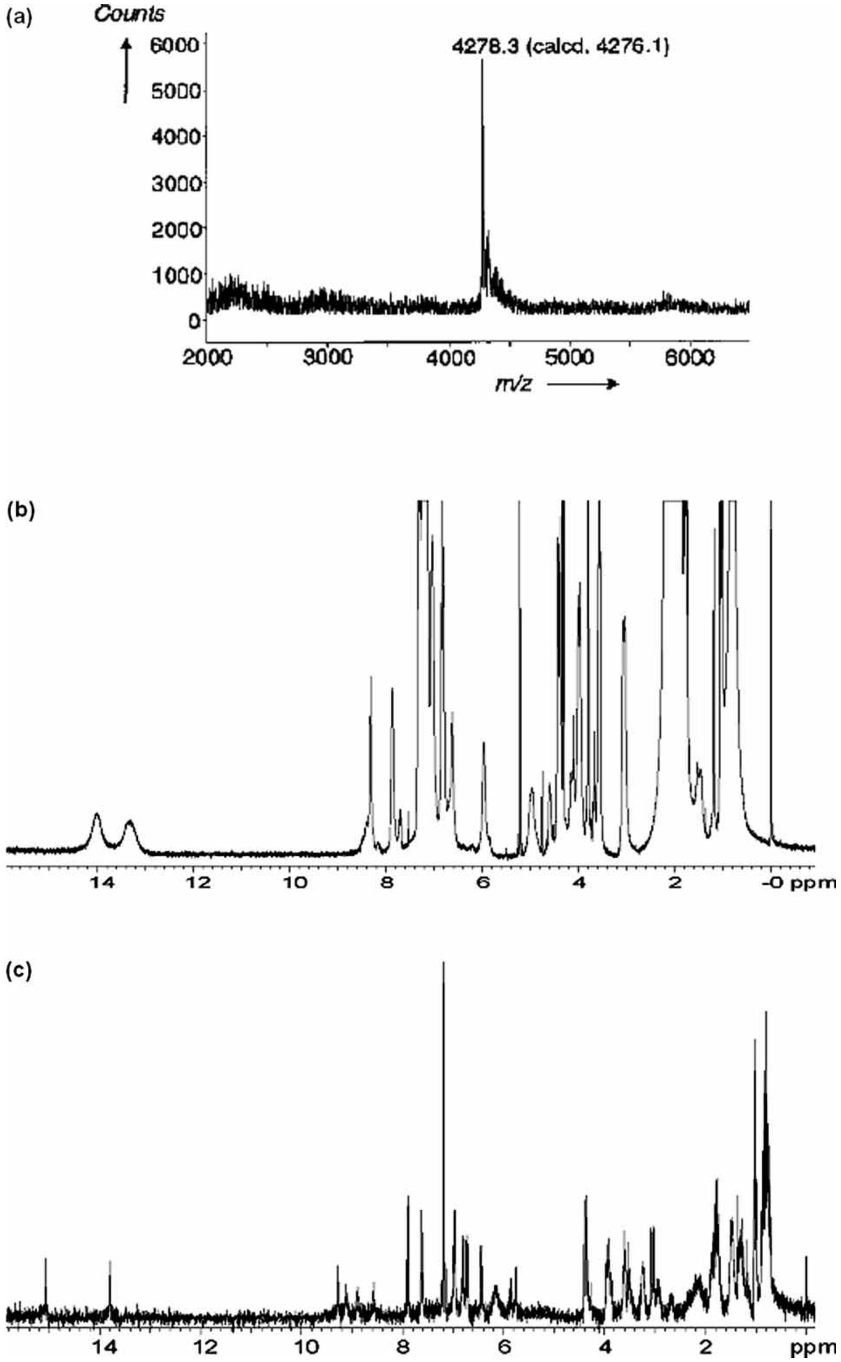

FIGURE 2 (a) MALDI-TOF MS spectrum of assembly $Ag^{+}\cdot[\mathbf{1a_3}\bullet(DEB)_6]^{18}$ and (b) ^{1}H NMR spectra of double rosette assemblies $[\mathbf{1a_3}\bullet(DEB)_6]$ and (c) $[\mathbf{1b_3}\bullet(CNPhCYA)_6]$ recorded at 300 K in $[D]^{8}$-toluene at 300 MHz.

AFM images in Fig. 3. In addition to the edge roughness, defects such as vacancies were not observed. Further, the substrate determines the alignment of the nanorod domains on surface (0°, 60°, 120°), which is related to the underlying three-fold symmetry of the HOPG lattice [49]. There are significant differences in the distribution of the nano-rod domains on the HOPG surfaces. In case of the assembly $Ag^{+}\cdot[\mathbf{1a}_3\bullet(DEB)_6]$ the domains are distinctly separated; while in case of the complex $Ag^{+}\cdot[\mathbf{1b}_3\bullet(CNPhCYA)_6]$ crossing of nanorod domains with different orientations creates extended and evenly distributed domain patterns. In both the cases the assemblies were oriented in the edge-on manner (Fig. 4). In edge-on fashion inter rosette spacings correspond to the width of double rosette molecular box; while height measurements correspond to the dimensions of the box face.

The roughness characterisation [34] of the observed jagged domain edges along the rows are

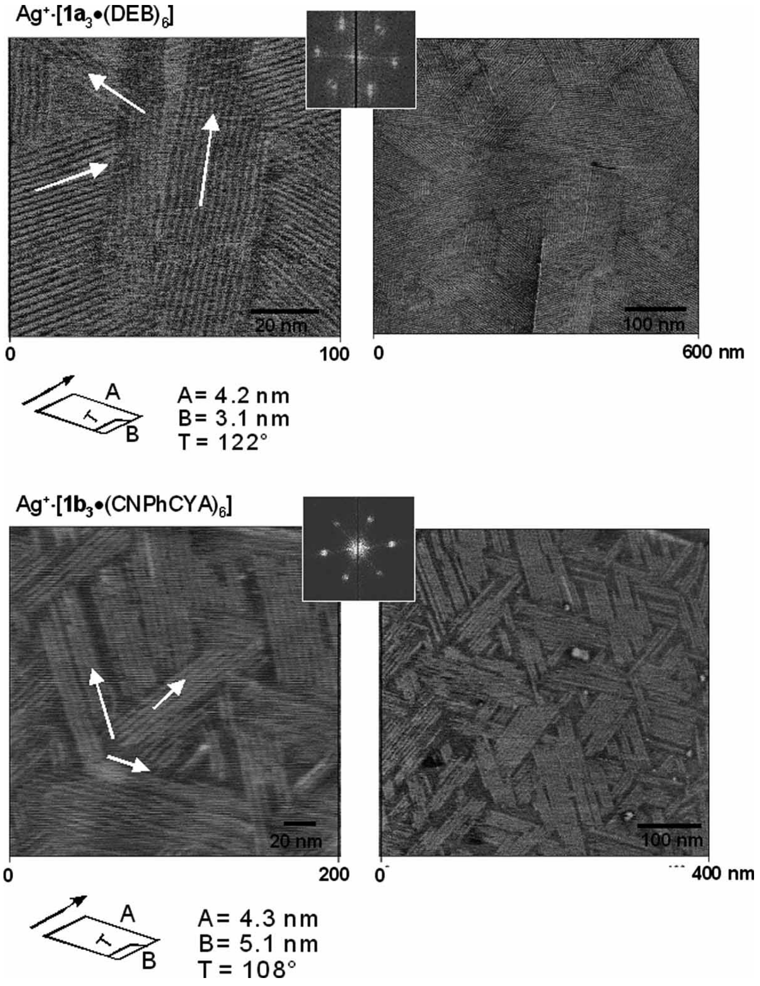

FIGURE 3 TM-AFM phase images of double rosette-silver complexes Ag$^+$·[**1b**$_3$•(DEB)$_6$] and Ag$^+$·[**1b**$_3$•(CNPhCYA)$_6$] on HOPG deposited in air. Inset shows 2-D FFT. Unit cell obtained from 2-D FFT's of high-resolution AFM images of the nanorod domains of rosettes are also shown. Arrows indicate the alignment of the nanorod domains according to the three-fold symmetry of the underlying graphite.

of 1.3(0.1) nm for assembly Ag$^+$·[**1b**$_3$•(DEB)$_6$] and 1.4(0.1) nm for assembly Ag$^+$·[**1b**$_3$•(CNPhCYA)$_6$] (Figs. 5 and 6), indicating the face to face stacking of double rosettes. In Figs. 5a and 5b the observed step lengths at the domain edges are plotted in the histograms for Ag$^+$·[**1b**$_3$•(DEB)$_6$] and Ag$^+$·[**1b**$_3$•(CNPhCYA)$_6$], respectively. In Fig. 6, the graphs of the peak positions observed in the histograms for different bin sizes are plotted versus the peak numbers, respectively. The linear regressions shows bin size-independent slopes. From the slopes integer spacings of differences along the rows of 1.3 ± 0.1 nm and 1.4 ± 0.1 nm were observed for assemblies Ag$^+$·[**1a$_3$**((DEB)$_6$] and Ag$^+$·[**1b$_3$**((CNPhCYA)$_6$], respectively. The spacings are comparable with the dimensions of individual rosette nanostructures [34] and suggest that the rosettes stack in the row direction.

The direct real-space observation of the individual rosettes comprising the nanorod domains was carried out in high-resolution AFM measurements. As shown in Fig. 3, the 2D fast Fourier transform (2-D FFT, inset in Fig. 3) shows reflections that correspond to the inter-row spacing. From an analysis of the 2-D FFTs, we obtained an oblique lattice structure, which is characterised by $a = 4.2(\pm 0.1)$ nm, b = 3.1(±0.1) nm and $\theta = 122(3)°$ for assembly Ag$^+$·[**1b**$_3$•(DEB)$_6$] and $a = 4.3$ (±0.1) nm, b = 5.1(±0.1) nm and $\theta = 108(3)°$ for assembly Ag$^+$·[**1b**$_3$•(CNPhCYA)$_6$]. Their unit cell probably contains three and four double rosette nanostructures, respectively, which corresponds to a formal area requirement of 5.0 nm^2/rosette and the gas-phase minimised structure possesses an area requirement of 3.64 nm^2/rosette [34]. These values are in good agreement with each other considering earlier reports of related double rosettes.

CONCLUSIONS

We have shown that silver atoms can be successfully incorporated into the self-assembled, hydrogen-bonded rosette assemblies based on substituted calix[4]arene dimelamine and barbiturate (cyanuric)

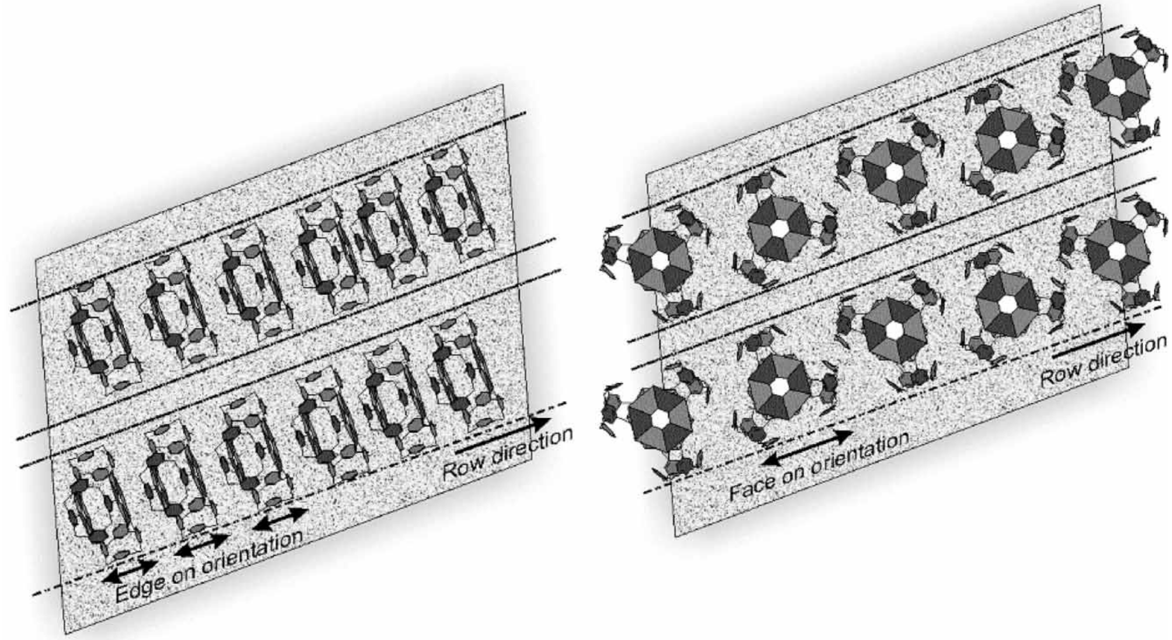

FIGURE 4 Double rosette assemblies Ag^{+}·[**1b**$_3$•(DEB)$_6$] and Ag^{+}·[**1b**$_3$•(CNPhCYA)$_6$], lie in edge-on fashion (left) rather than in face-on fashion (right). The double rosette is a *box-like* structure; edge-on orientation denotes lying of the boxes with edges anchored and flat-surfaces vertically positioned; while face-on indicates anchoring of the flat-surfaces. This is well indicated by the height values: 4.6 ± 0.1 nm for Ag^{+}·[**1a**$_3$•(DEB)$_6$] and 4.3 ± 0.1 nm for Ag^{+}·[**1b**$_3$•(CNPhCYA)$_6$], which correspond to the lateral dimensions of the *box*-face. (Substituents on the assemblies and metal atoms are not shown for clarity).

acid moieties. The rosettes formed in solution are very stable and can be deposited onto solid surfaces to create metal-containing supramolecular aggregates with nano-sized dimensions ranging from 0-D (individual rosettes) to 2-D (rosette layers). In these highly ordered nanorod domains, face-to-face stacked rosettes form parallel rows lying in edge-on fashion on HOPG surface. Our results show the feasibility of self-assembled hydrogen-bonded assemblies to serve as a scaffold for the formation of metal containing nanorod arrays. Further, platinated and copper functionalised double rosette assemblies can be similarly obtained as these cations also show complexation with rosette structures [44]. Thus, the strategy reported here may constitute a viable route for the bottom–up fabrication of, for example, conducting nanowires templated by hydrogen-bonded assemblies.

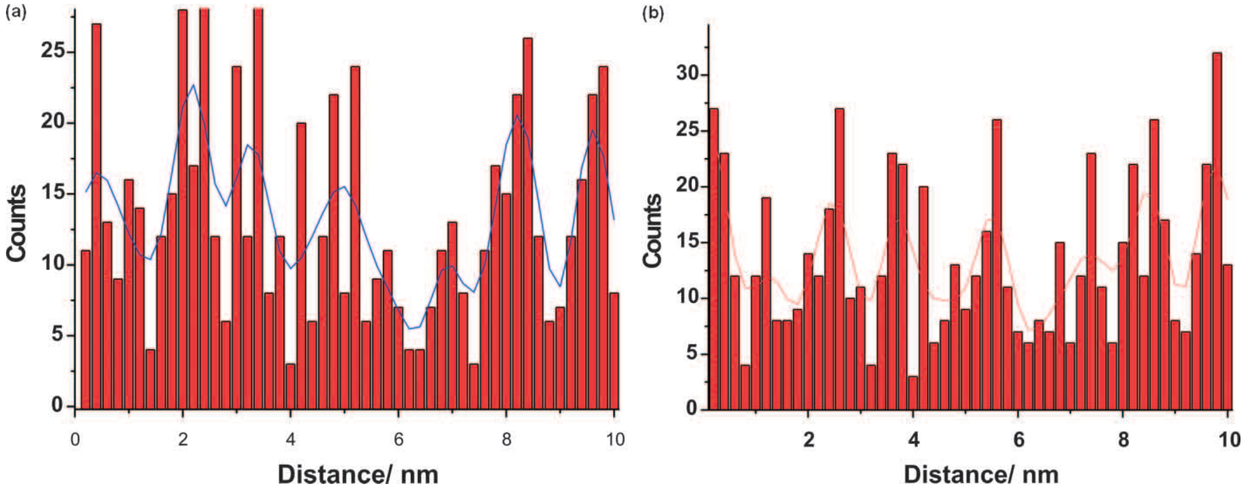

FIGURE 5 Histograms of the observed distance-differences at the edge of nanorod domains obtained by AFM analysis for (a) Ag^{+}·[**1a**$_3$•(DEB)$_6$] (0.25 nm bin size) and (b) Ag^{+}·[**1b**$_3$•(CNPhCYA)$_6$] (0.20 nm bin size) with Fourier smoothened data (solid lines).

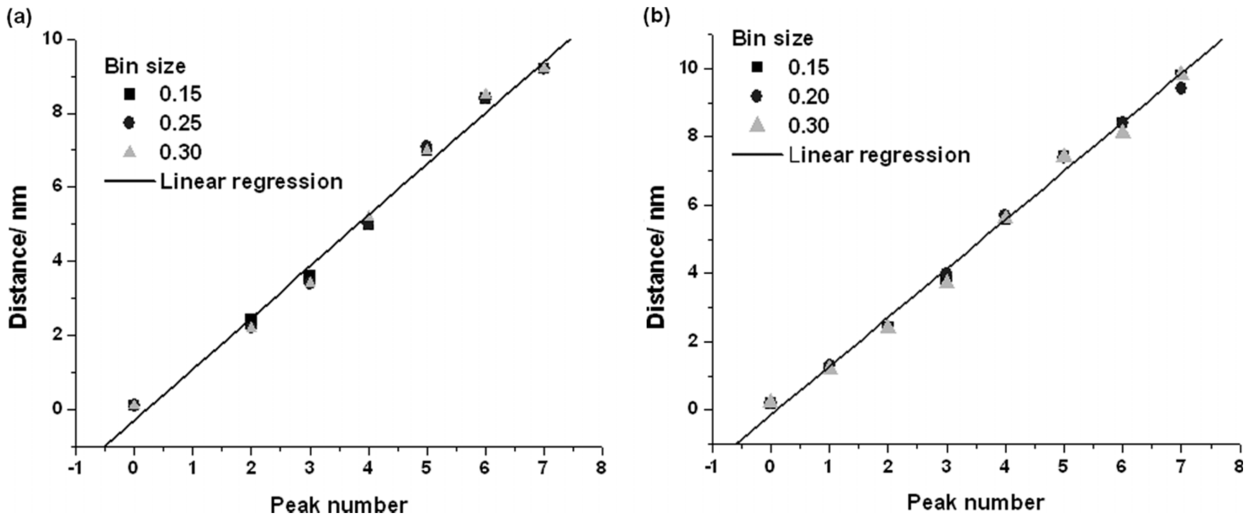

FIGURE 6 Plots of observed distance-differences at the edge of nanorod domains for different bin sizes versus peak number in the histograms analysed. From the slopes, the integer spacings of the distance differences are determined for (a) Ag$^+$·[**1a$_3$**•(DEB)$_6$] and (b) Ag$^+$·[**1b$_3$**•(CNPhCYA)$_6$].

Acknowledgements

This work has been financially supported by ESF–SONS-FunSMARTs project.

References

[1] Balzani, V.; Credi, A.; Venturi, M. *Chem. Eur. J.* **2002**, *8*, 5524.
[2] Service, R. F. *Science* **2001**, *293*, 782.
[3] Whitesides, G. M.; Love, J. C. *Sci. Am.* **2001**, *285*, 32.
[4] Peercy, P. S. *Nature* **2000**, *406*, 1023.
[5] Ito, T.; Okazaki, S. *Nature* **2000**, *406*, 1027.
[6] Walraff, G. M.; Hinsberg, W. D. *Chem. Rev.* **1999**, *99*, 1801.
[7] Supramolecular Chemistry and Self-Assembly, *Science* **2002**, *295*, 2400.
[8] Huang, Y.; Duan, X. F.; Cui, Y.; Lauhon, L. J.; Kim, K. H.; Lieber, C. M. *Science* **2001**, *294*, 1313.
[9] Postma, H. W. C.; Teepen, T.; Yao, Z.; Grifoni, M.; Dekker, C. *Science* **2001**, *293*, 76.
[10] Sone, E. D.; Zubarev, E. R.; Stupp, S. I. *Angew. Chem., Int. Ed.* **2002**, *41*, 1705.
[11] Feldheim, D. L.; Keating, C. D. *Chem. Soc. Rev.* **1998**, *27*, 1.
[12] Tsai, C. J.; Ma, B. Y.; Kumar, S.; Wolfson, H.; Nussinov, R. *Crit. Rev. Biochem. Mol. Biol.* **2001**, *36*, 399.
[13] Vilar, R. *Supramol. Assembly Via Hydrogen Bonds II* **2004**, *111*, 85.
[14] Elemans, J.; Rowan, A. E.; Nolte, R. J. M. *J. Mater. Chem.* **2003**, *13*, 2661.
[15] Keizer, H. M.; Sijbesma, R. P. *Chem. Soc. Rev.* **2005**, *34*, 226.
[16] Balzani, V.; Credi, A.; Raymo, F. M.; Stoddart, J. F. *Angew. Chem. Int. Ed.* **2000**, *39*, 3348.
[17] Aviram, A.; Ratner, M.; Eds.; *Molecular Electronics: Science and Technology*; New York Academy of Sciences: New York, 1998.
[18] Ball, P. *Nature* **2000**, *406*, 118.
[19] Reed, M. A.; Tour, J. M. *Sci. Am.* **2000**, *June*, 68.
[20] Yokoyama, T.; Yokoyama, S.; Kamikado, T.; Okuno, Y.; Mashiko, S. *Nature* **2001**, *413*, 619.
[21] De Feyter, S.; De Schryver, F. C. *Chem. Soc. Rev.* **2003**, *32*, 139.
[22] Gimzewski, J. K.; Joachim, C. *Science* **1999**, *283*, 1683.
[23] Barth, J. V.; Costantini, G.; Kern, K. *Nature* **2005**, *437*, 671.
[24] Barth, J. V.; Weckesser, J.; Cai, C.; Günter, P.; Bürgi, L.; Jeandupeux, O.; Kern, K. *Angew. Chem., Int. Ed.* **2000**, *39*, 1230.
[25] Auletta, T.; Dordi, B.; Mulder, A.; Sartori, A.; Onclin, S.; Bruinink, C. M.; Nijhuis, C. A.; Beijleveld, H.; Péter, M.; Schönherr, H.; Vancso, G. J.; Casnati, A.; Ungaro, R.; Ravoo, B. J.; Huskens, J.; Reinhoudt, D. N. *Angew. Chem., Int. Ed.* **2004**, *43*, 369.
[26] Joachim, C.; Gimzewski, J. K.; Aviram, A. *Nature* **2000**, *408*, 541.
[27] Jackel, F.; Watson, M. D.; Mullen, K.; Rabe, J. P. *Phys. Rev. Lett.* **2004**, *92*, 188303.
[28] Maoz, R.; Frydman, E.; Cohen, S. R.; Sagiv, J. *Adv. Mater.* **2000**, *12*, 725.
[29] Samori, P. *Chem. Soc. Rev.* **2005**, *34*, 551.
[30] Böhringer, M.; Morgenstern, K.; Schneider, W. D.; Berndt, R.; Mauri, F.; De Vita, A.; Car, R. *Phys. Rev. Lett.* **1999**, *83*, 324.
[31] Dmitriev, A.; Lin, N.; Weckesser, J.; Barth, J. V.; Kern, K. *J. Phys. Chem. B* **2002**, *106*, 6907.
[32] Klok, H. A.; Jolliffe, K. A.; Schauer, C. L.; Prins, L. J.; Spatz, J. P.; Moller, M.; Timmerman, P.; Reinhoudt, D. N. *J. Am. Chem. Soc.* **1999**, *121*, 7154.
[33] Schönherr, H.; Paraschiv, V.; Zapotoczny, S.; Crego-Calama, M.; Timmerman, P.; Frank, C. W.; Vancso, G. J.; Reinhoudt, D. N. *Proc. Natl Acad. Sci. USA* **2002**, *99*, 5024.
[34] van Manen, H. J.; Paraschiv, V.; Garcia-Lopez, J. J.; Schönherr, H.; Zapotoczny, S.; Vancso, G. J.; Crego-Calama, M.; Reinhoudt, D. N. *Nano Lett.* **2004**, *4*, 441.
[35] Friggeri, A.; Van Manen, H.-J.; Auletta, T.; Li, X.-M.; Zapotoczny, S.; Schönherr, H.; Vancso, G. J.; Huskens, J.; Van Veggel, F. C. J. M.; Reinhoudt, D. N. *J. Am. Chem. Soc.* **2001**, *123*, 6388.
[36] Zander, C.; Enderlein, J.; Keller, R. A.; Eds.; *Single Molecule Detection in Solution*; Wiley-VCH: Berlin, 2002.
[37] Ambrose, W. P.; Goodwin, P. M.; Jett, J. H.; Van Orden, A.; Werner, J. H.; Keller, R. A. *Chem. Rev.* **1999**, *99*, 2929.
[38] Fotiadis, D.; Scheuring, S.; Müller, S. A.; Engel, A.; Müller, D. J. *Micron* **2002**, *33*, 385.
[39] Mörner, W. E.; Orrit, M. *Science* **1999**, *283*, 1670.
[40] Prins, L. J.; Reinhoudt, D. N.; Timmerman, P. *Angew. Chem., Int. Ed.* **2001**, *40*, 2382.
[41] Braun, E.; Eichen, Y.; Sivan, U.; Ben-Yoseph, G. *Nature* **1998**, *391*, 775.
[42] Reches, M.; Gazit, E. *Science* **2003**, *300*, 625.
[43] Jolliffe, K. A.; Crego-Calama, M.; Fokkens, R.; Nibbering, N. M. M.; Timmerman, P.; Reinhoudt, D. N. *Angew. Chem., Int. Ed.* **1998**, *37*, 1247.
[44] Timmerman, P.; Jolliffe, K. A.; Crego-Calama, M.; Weidmann, J.-L.; Prins, L. J.; Cardullo, F.; Snellink-Rueel, B. H. M.;

Fokkens, R. H.; Nibbering, N. M. M.; Shinkai, S.; Reinhoudt, D. N. *Chem. Eur. J.* **2000**, *6*, 4104.

[45] Timmerman, P.; Vreekamp, R. H.; Hulst, R.; Verboom, W.; Reinhoudt, D. N.; Rissanen, K.; Udachin, K. A.; Ripmeester, J. *Chem. Eur. J.* **1997**, *3*, 1823.

[46] Karas, M.; Bachmann, D.; Bahr, U.; Hillenkamp, F. *Int. J. Mass Spectrom. Ion Proc.* **1987**, *78*, 53.

[47] Hillenkamp, F.; Karas, M. *Anal. Chem.* **1991**, *6*, 1193A.

[48] Schönherr, H.; Crego-Calama, M.; Vancso, G. J.; Reinhoudt, D. N. In *Encyclopedia of Nanoscience and Nanotechnology*; Schwarz, J. A., Contescu, C., Putyera, K., Eds.; Marcel Dekker: New York, 2004.

[49] # There is also 6° deviation between two neighboring nanorod domains. This is because these assemblies show supramolecular chirality (*D*3 symmetry). Due to the lack of any chiral centre in the assemblies these assemblies are present in the form of two enantiopure domains, which show spontaneous resolution of racemic mixture of *P* and *M* rosettes.
Prins, L.J. PhD Thesis, University of Twente, 2001.